# Combustion performance of plasma-stabilized lean flames in a gas turbine model combustor

Victorien P Blanchard, Philippe Scouflaire, Christophe O Laux, Sebastien Ducruix

Applications in Energy and Combustion Science 15 (2023) 100158

Contents lists available at ScienceDirect

Applications in Energy and Combustion Science

journal homepage: www.sciencedirect.com/journal/applications-in-energy-and-combustion-science

# Combustion performance of plasma-stabilized lean flames in a gas turbine model combustor

Victorien P. Blanchard *, Philippe Scouflaire, Christophe O. Laux, Sébastien Ducruix

*Laboratoire EM2C, CNRS-CentraleSupélec, Université Paris-Saclay, Gif-sur-Yvette, France*

ARTICLE INFO

*Keywords:*
Plasma-assisted combustion
Gas turbine model combustor
Nanosecond repetitively pulsed discharges
Lean extinction
$NO_X$ reduction

ABSTRACT

This work presents an experimental study of the stabilization of lean methane-air flames by nanosecond repetitively pulsed (NRP) discharges. The experimental facility consists of a gas turbine model combustor with a Lean-Premixed-Prevaporized injector. The working pressure is 1 atm. The fuel is injected through two stages, each stabilized by swirl. The main stage consists of a multipoint annular injection. This facility is representative of a single sector of a gas turbine combustion chamber. The NRP discharges significantly extend the lean blow-off limit for a wide range of operating conditions, down to an equivalence ratio of 0.16. Lean flame stabilization is demonstrated for flame thermal powers up to 100 kW, with an electric power of less than 0.2% of the flame thermal power. We also observe plasma-assisted lean flames emiting less $NO_X$ than the leanest stable flames without plasma. Finally, by exploring the application of various pulse patterns instead of applying the discharges continuously at a constant repetition frequency, the plasma-to-flame power ratio required to stabilize a lean flame is decreased to 0.06% and the pollutant emissions can be further decreased.

## 1. Introduction

The development of combustion chambers for future gas turbines and, more specifically, aircraft engines is driven by the reduction of $NO_X$, particulate matters, CO, and unburnt hydrocarbons (UHC) emissions, the ability to reignite in severe conditions (mainly high-altitude and cold environment), the improvement of combustion efficiency, and the mitigation of combustion instabilities. One strategy to tackle these challenges is to operate in the lean premixed combustion regime. It involves the design of new injector technologies with efficient fuel-air mixing and the use of a swirling flow to stabilize the flame aerodynamically [1]. Engine manufacturers and academic communities have proposed various geometries and injection strategies [1]. For example, fuel injection in a crossflow of air can efficiently mix fuel and air [2–4]. To control combustion instabilities, staged injection of fuel and air has also been investigated [5–7]. This enables flexibility and modulation of the local equivalence ratios and the flow conditions to ensure flame holding. Despite the progress made to control lean premixed combustion through injector design, these flames are still prone to instability and extinction [1].

Plasma discharges have produced remarkable results to sustain the efficient combustion of lean flames [8,9]. In particular, Nanosecond Repetitively Pulsed (NRP) discharges [10] are a promising candidate for plasma-assisted combustion in practical applications because they produce high amounts of radicals with a very low power budget [11,12]. Laboratory-scale burners dedicated to plasma-assisted combustion usually operate at low power, and only a few studies have focused on swirl-stabilized burners. Barbosa *et al.* [13] showed that NRP discharges applied at 30 kHz could drastically extend the lean blow-off (LBO) limit of propane-air flames up to 50 kW. These results were then extended to methane-air flames [14]. Xiong *et al.* [15] also showed that NRP discharges can stabilize the second-stage chamber of a 50-kW sequential burner with only 100 W of plasma power. Lacoste *et al.* [16] showed that NRP discharges can suppress self-sustained thermo-acoustic instabilities in a lean, premixed, methane-air, swirl-stabilized burner of thermal power equal to 4 kW. Moeck et al. [17] demonstrated that NRP discharges can reduce the noise level by a factor of 5 in a 43-kW lean premixed natural gas-air flame. However, depending on the conditions, they also observed that the discharges may promote flame oscillations. The mitigation of the thermo-acoustic instabilities of a 14-kW, swirl-stabilized, methane-air flame was also achieved by Shanbhogue *et al.* [18] using NRP discharges. They further developed an open-loop control system of the pressure amplitude in the combustion chamber based on the discharge repetition frequency. The effect of pressure on plasma-assisted flames was studied by Di Sabatino and Lacoste [19].

* Corresponding author.
*E-mail address:* victorien.blanchard@centralesupelec.com (V.P. Blanchard).

https://doi.org/10.1016/j.jaecs.2023.100158
Received 3 April 2023; Received in revised form 1 June 2023; Accepted 6 June 2023
Available online 7 June 2023

**Nomenclature**

| | |
|---|---|
| BVB | Bubble Vortex Breakdown |
| CRZ | Central Recirculation Zone |
| CVB | Conical Vortex Breakdown |
| ISL | Inner Shear Layer |
| LBO | Lean Blow-Off |
| LPP | Lean Premixed Prevaporized |
| NRP | Nanosecond Repetitively Pulsed |
| OSL | Outer Shear Layer |
| THC | Total Hydrocarbon Content |
| $f_R$ | Pulse repetition frequency |
| $N_{ON}$ | Number of discharges in a burst |
| $N_{OFF}$ | Number of periods between two consecutive bursts |
| $P_{flame}$ | Flame thermal power |
| $P_{plasma}$ | Plasma electric power |
| $r_{DC}$ | Duty cycle ratio |
| $\alpha$ | Fuel staging factor |
| $\Phi_g$ | Global equivalence ratio |
| $\Phi_p$ | Pilot-stage local equivalence ratio |
| $\Phi_m$ | Multipoint-stage local equivalence ratio |
| $\Phi_{LBO}$ | Global equivalence ratio at blow-off |
| $\Phi_{LBO\text{-}p}$ | Global equivalence ratio at blow-off with plasma |
| $\Phi_{LBO\text{-}wo}$ | Global equivalence ratio at blow-off without plasma |

They used NRP discharges to extend the stability domain and the LBO limit of swirl, premixed, methane-air flames at pressures up to 5 bar for flame thermal powers varying between 5 and 20 kW. Vignat *et al.* [20] investigated the ability of NRP discharges to extend the LBO limit of liquid fuels. Using a single swirl-stabilized 5-kW burner at atmospheric pressure, they performed experiments with perfectly premixed methane-air and with sprays of liquid heptane and liquid dodecane. A substantial extension of the LBO limit for the three fuels was obtained with NRP discharges showing that the beneficial effects on the LBO extension obtained in gaseous hydrocarbon mixtures can also be obtained with spray burners. Finally, Kim *et al.* [21] demonstrated that a change in flame shape induced by NRP discharges significantly reduces pressure fluctuations in the combustion chamber. An active control scheme was developed with promising results. They also showed that the combustion efficiency of plasma-assisted lean, premixed, methane-air, 6-kW flames was increased by 10% with a minimal $NO_X$ penalty. This represents a gain of 500 W of flame thermal power for an electric power input of only 30 W.

The combustion efficiency and the pollutant emissions of lean flames stabilized by NRP discharges were characterized in several studies [15, 21–25]. For the conditions of these studies, the $NO_X$ emissions increased when the NRP discharges were applied. The CO emissions did not increase in Refs. [23,24]. Due to improved combustion efficiency, Choe & Sun [25] measured a reduction of CO emissions when NRP discharges were applied. Moreover, it was shown in Refs. [22–24] that the level of $NO_X$ emitted by plasma-assisted flames was lower than that of $NO_X$ emitted in pure air with the same NRP discharges. This trend, however, was not confirmed by Choe & Sun.

Several parameters of the NRP discharges can influence $NO_X$ emissions. Lacoste *et al.* [24], Kim *et al.* [21], and Xiong *et al.* [15] measured a linear increase of $NO_X$ emissions with the discharge repetition frequency. Choe & Sun did not observe a significant effect of the repetition frequency, but the range of repetition frequencies tested was narrow. $NO_X$ emissions also increase with the peak voltage and, at a constant air flow rate, with the plasma electric power [15,21,25]. Lacoste *et al.* varied the air flow rate and showed that $NO_X$ emissions linearly increase with the plasma power per unit mass of air injected in the combustor. In contrast, according to Choe & Sun, $NO_X$ emissions divided by the plasma power are governed mainly by the pulse peak voltage rather than the pulse repetition frequency due to the plasma chemistry, which is more sensitive to the reduced electric field. The sensitivity of $NO_X$ emissions to the different parameters discussed above depends on the range of variation of these parameters, the type of burner, and the location of the NRP discharges. Additional studies are thus needed to draw general conclusions.

One of the goals of plasma-assisted combustion is to stabilize lean flames with low $NO_X$ emissions. However, when applying NRP discharges in premixed methane-air flames, Refs. [23] and [24] showed that the level of $NO_X$ remained constant for equivalence ratios from 1 to 0.7. In Ref. [25], the authors observed a similar plateauing value for equivalence ratios between 0.75 and 0.55 and a lower plateauing value for equivalence ratios from 0.4 to 0.2. This suggests that reducing the $NO_X$ emissions of plasma-assisted flames at very low equivalence ratios is possible. However, the combustor in Ref. [25] was operated at a flame thermal power of less than 5 kW. The objective of the present work is to assess the ability of NRP discharges to stabilize lean flames in a combustor more representative of a gas turbine engine at much higher power and to characterize pollutant emissions and combustion efficiency.

This paper is organized as follows: Section 2 describes the combustor and the experimental approach. Then, in Section 3, the LBO limit of various flames without and with plasma is characterized. Subsequently, the combustion performance of these flames near blow-off are measured in Section 4. And finally, we explore the impact of the pulse pattern on the stability and $NO_X$ emissions of a 50-kW lean flame in Section 5.

## 2. Experimental setup and lean flame characterization methods

### 2.1. Gas turbine model combustor for plasma-assisted combustion: BIMER-PAC facility

The burner consists of a plenum, an injector, and a combustion chamber with a square cross-section of 15-cm width and 50-cm length. The burner is shown in Fig. 1. It is dedicated to plasma-assisted combustion studies and has been duplicated from the BIMER testbench [26–28]. The burner is operated at atmospheric pressure. The chamber backplane and its upper and lower walls are water-cooled to ensure thermal equilibrium when operating in steady state. K-type thermocouples are mounted in the water-cooling circuit of each wall to monitor the temperature and to determine the heat flux extracted at the walls. Each water-cooled wall has an independent cooling circuit. The side walls are made of silica to provide wide optical access and continuous

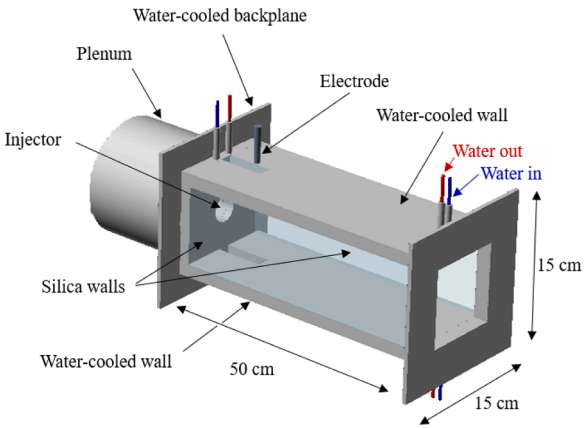


**Fig. 1.** Combustor of the BIMER-PAC facility; adapted from [28].

monitoring of the flame. Two small silica windows facing each other are inserted in the upper and lower walls close to the injector for laser diagnostics. A thermocouple is inserted in the injector downstream of the multipoint stage swirling vane to detect flame flashback. To monitor the wall surface temperature, two thermocouples are integrated into the lower wall via blind holes. The thermocouples are recessed 1 mm from the inner surface of the wall to prevent them from receiving radiation from the flame. They are located on the centerline of the wall at 25 cm and 42 cm from the chamber backplane, respectively.

The staged injector mounted in the combustor is shown in Fig. 2(a). It comprises a pilot stage with a central injection tube (4 mm in diameter) to inject a non-swirling inner jet of fuel, and the associated radial swirler for air (geometrical swirl number of 1). This stage creates a fuel-rich region to anchor the flame. The outer stage of the injector is an annular multipoint stage where the fuel is fed through 15 equally spaced holes (0.7 mm in diameter) in a crossflow of air downstream of a second radial swirler (geometrical swirl number of 0.9) to enable efficient turbulent mixing of fuel and air. This stage is meant to operate in lean premixed conditions. The swirlers of the two stages are arranged in a co-rotating orientation. This Lean Premixed Prevaporized (LPP) injector design provides realistic air-fuel injection and an engine-like recirculation zone in the combustion chamber. In this study, we use gaseous methane. The methane flow rate in each stage is independently controlled to vary the fuel staging factor (Bronkhorst Cori-Flow M55-RAD-44-0-S, Bronkhorst EL-Flow F-203AC-AAD-44-V). The fuel staging factor, α, is defined as the ratio of the fuel mass flow rate injected through the pilot stage to the total fuel mass flow rate.

$$\alpha = \frac{\dot{m}_{CH_4,pilot}}{\dot{m}_{CH_4,multi} + \dot{m}_{CH_4,pilot}} \quad (1)$$

where $\dot{m}_{CH_4,pilot}$ and $\dot{m}_{CH_4,multi}$ are the methane mass flow rates through the pilot and multipoint stages, respectively. A single mass flow controller controls the total air flow rate. Air is fed in the plenum and naturally splits, thanks to head losses, into a 20-80% distribution between the pilot (20%) and multipoint (80%) swirlers [26]. Depending on the air flow rate, we use either a mass flow controller with a full scale of 200 $Nm^3 \cdot h^{-1}$ (Bronkhorst EL-Flow F-206BI-FA-00-V) or a mass flow controller with a full scale of 600 $Nm^3 \cdot h^{-1}$ (Bronkhorst MassStream D-6391-DR/003BI). The global equivalence ratio, denoted $\Phi_g$, is defined as the total methane-to-air mass flow rate ratio divided by the stoichiometric methane-to-air mass flow rate ratio. Given the air distribution between the two stages and the fuel staging factor, we define the local equivalence ratios $\Phi_p$ and $\Phi_m$ for the pilot stage and the multipoint stage, respectively:

$$\Phi_p = 5\alpha\Phi_g \quad (2)$$

$$\Phi_m = 1.25(1-\alpha)\Phi_g \quad (3)$$

To give an idea, the bulk velocity at the injector outlet is about 16 m. $s^{-1}$ for a 50-kW flame at an equivalence ratio of 0.5.

As shown in Fig. 2(a), the nanosecond discharges are produced in a pin-to-ring configuration between the high-voltage anode and the rim of the divergent portion of the pilot stage, which is grounded. The inter-electrode gap is approximately 7 mm. The electrode body is water-cooled and made of stainless steel; the tip is made of tungsten. The electrode is inserted through the upper wall of the combustion chamber. At the passage point, the electrode is insulated from the body of the combustor with a boron nitride jacket. The pulses are applied at repetition frequencies between 33 kHz and 77 kHz, with a maximal energy input per pulse of 4 mJ delivered by a 10-ns-duration high-voltage pulse generator (FID Technology 15-100NM10). A photograph of the NRP discharges in Fig. 2(b) shows that they appear in the form of filaments. Visual observations indicate that the discharges are rotating because of the swirl motion of the flow, but they cover less than half the ring defined by the rim of the divergent portion of the pilot stage. The NRP discharges in this experiment are either nonequilibrium sparks [10] or thermal sparks [29], further investigations are needed to determine the exact regime.

An ICCD camera (Princeton Instruments, PI-MAX 4) fitted with a 50-mm lens (Nikon, AF Nikkor f/1.4) and a bandpass filter (Asahi spectra, F0101, CWL = 430 nm) centered on the CH* chemiluminescent emission is used for flame imaging. The images presented in this article were recorded with a gate width of 200 μs, integrated along the line of sight, and averaged over 200 samples.

### 2.2. Discharge electrical characterization

Voltage and current traces are measured with electrical probes (Lecroy PPE 20kV, Pearson current monitor model 6585) connected to an oscilloscope (TeledyneLecroy HDO 6104) to monitor the energy input of each discharge. The probes are located halfway along the coaxial cable using the configuration detailed in our previous work [30]. An example of typical voltage, current, and energy traces is plotted in Fig. 3. The pulse generator delivers a first pulse with an amplitude of approximately 4 kV. Due to the impedance mismatch at the electrode between the coaxial cable and the interelectrode gap, the pulse is partially

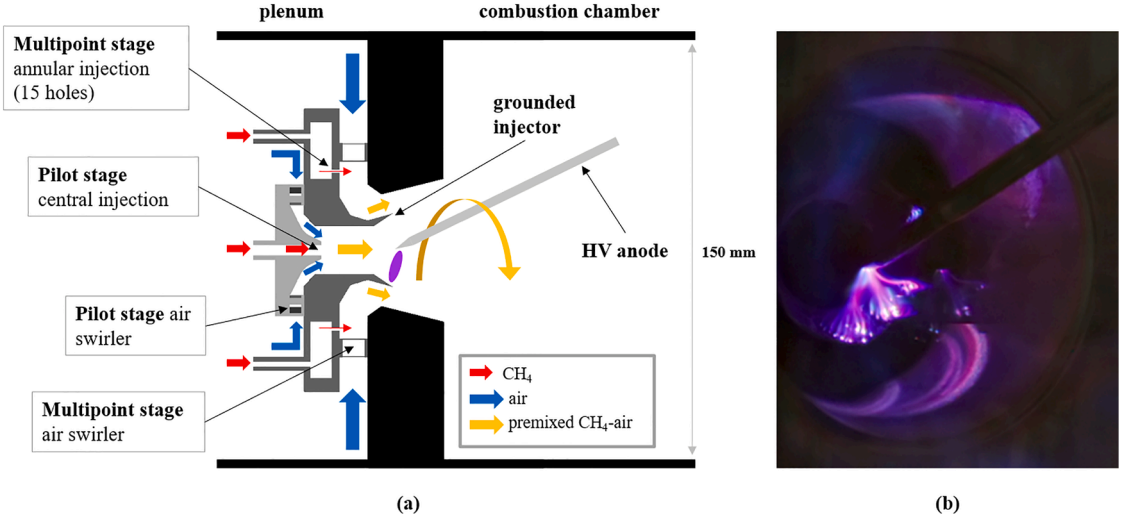


**Fig. 2.** (a) Schematic of the two-stage injector with the high-voltage electrode assembly. (b) Close-up photograph of the injector with NRP discharges applied in a 60-kW flame. Credits: Auguste & Louise SARL.

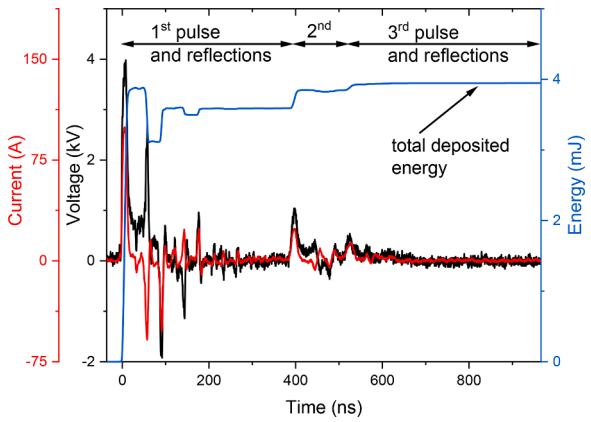


**Fig. 3.** Typical voltage, current, and energy traces measured during the experiments.

reflected, meaning that the peak voltage at the electrode is doubled compared to the value measured halfway along the coaxial cable in Fig. 3. The reflection travels back to the pulse generator where it is again reflected. Therefore, the initial energy amplitude at about 20 ns corresponds to the energy of the incident pulse, but not all of this energy is deposited due to the reflection. The reflected pulse traveling back from the electrode to the pulser carries energy and it passes the electrical probes again. The reflected energy is subtracted from the initial energy of the incident pulse to give the net balance of energy deposited in the plasma. The reflection and the remote measurement explain the non-monotonic energy evolution (if the electrical probes were close to the electrode, we would only observe a build-up of deposited energy). A few reflections at the electrode and at the pulse generator output are necessary to deposit all the energy. Note, however, that 75% of the energy is deposited by the first incident pulse. We also observe a second and a third pulse at 400 and 550 ns due to the pulse generator hardware. These secondary pulses deposit less than 10% of the total discharge energy. The energy values and their standard deviations reported in this work are obtained by averaging over about 1000 pulses and the average plasma electric power, $P_{plasma}$, is obtained by multiplying the total energy deposited by the repetition frequency of the NRP discharges.

Fig. 3 also shows that the energy of the first incident pulse is 3.9 mJ, and 3.1 mJ are deposited. The energy coupling is thus about 80%. The reflection of the first pulse has also an energy coupling of about 80%. Then, the subsequent reflections and pulses have an energy coupling close to 100% due to better impedance matching.

### 2.3. Lean blow-off limit determination

To determine the LBO limit of the burner at constant thermal power $P_{flame}$, defined as the fuel mass flow rate multiplied by the fuel heating value, we proceed as follows. First, we ignite a low-power flame, and then we increase the flame power up to the targeted power at an equivalence ratio of 0.8 (or higher if the flame is unstable). To ensure reproducibility, this operating condition is maintained until the wall surface temperature, measured with thermocouples, reaches steady state. Then, keeping the methane flow rates constant, the air flow rate is gradually increased to reduce the equivalence ratio until extinction. This procedure is repeated 5 to 10 times for each operating condition studied. To investigate the influence of the plasma on the lean blow-off, we first determine the limit without plasma and then with NRP discharges. The water-cooled electrode is always present in the chamber, whether the plasma is applied or not.

### 2.4. Gas analysis at the chamber outlet

A gas sampling probe is installed at the exit of the combustion chamber and connected to commercial gas analyzers via a heated line to measure the combustion products. A first gas analyzer (SK-electroniks UPAS-FID) comprises a flame ionization detector to measure the total hydrocarbon content (THC), and electrochemical cells for $CH_4$. A second gas analyzer (Horiba VA-5000) measures $CO_2$, CO, NO, and $N_2O$ based on non-dispersive infrared absorption spectroscopy, $O_2$ with a paramagnetic cell, and $NO_2$ with electrochemical cells. All data are monitored and recorded by a computer. To prevent interference from $H_2O$, water vapor is removed with a cold trap bath from the gas stream before entering the second analyzer. This gas analyzer measures mole fractions in the dried gases. The procedure to deduce the mole fraction of $H_2O$ and to infer the actual mole fractions of all the species as well as the combustion efficiency $\eta_c$, is presented in Ref. [31]. The combustion efficiency, $\eta_C$, is derived from the CO and unburnt gases measured at the combustion chamber outlet. It corresponds to the ratio of the measured enthalpy variation based on the chemical composition to the enthalpy variation that would be obtained if the combustion were complete (i.e., if the combustion products consisted only of $CO_2$ and $H_2O$). It is, therefore, a measure of the actual heat release divided by the theoretical heat release.

We also performed in Ref. [31] a 25-point mapping at the combustor exit plane to assess the homogeneity of the burnt gases. We showed that the burnt gases are homogeneously mixed in the extraction plane. In the present work, the gas sampling probe is thus installed at the center point of the outlet plane of the combustion chamber.

Gas analysis is carried out as follows during the experiments. Once the flame is set to the chosen operating conditions, we start the acquisitions after a delay corresponding to the suction of the gas in the sampling line. By monitoring the temporal evolution of the measurements, we ensure that the acquisition starts once steady state is reached. Then, measurements are acquired during at least one minute and are temporally averaged. The analyzers are calibrated with commercial bottles of known gas composition matching the scales of the analyzers.

## 3. Lean blow-off extension with NRP discharges

In previous work, Barbosa *et al.* [13] used a similar burner with a two-stage multipoint injector. They showed that it is possible to extend the LBO limit of a propane-air flame with NRP discharges, and they succeeded in sustaining lean flames down to a global equivalence ratio of 0.11. However, the equivalence ratio was reduced by decreasing the fuel flow rate. Hence, the flame thermal power was reduced accordingly during the experiments and remained below 50 kW. At the lean blow-off limit with plasma, the flame power was thus only 12 kW. Furthermore, most experiments were carried out with a fuel staging factor of 100% (pilot-only fuel injection). Although these plasma-assisted combustion results are promising for practical applications, more work is needed. In particular, it is essential to investigate higher flame thermal powers and other fuel staging conditions. This is the objective of the present section.

### 3.1. Study of the extinction sequence without and with NRP discharges

A typical LBO sequence without plasma is represented in Fig. 4. At 50 kW and $\alpha = 40\%$, the equivalence ratio is decreased by increasing the air flow rate while keeping the methane flow rate constant, i.e., keeping a constant thermal power. At $\Phi_g = 0.68$, we observe a stable V-shape flame. As the equivalence ratio is decreased, the emission of the flame is less intense, but the flame is still in a stable V-shape until $\Phi_g = 0.60$. Then, the flame starts oscillating and abruptly blows off at $\Phi_g = 0.56$. This extinction sequence is reproducible and consistently exhibits the same characteristics.

The V-shape flame is commonly observed in swirl-stabilized combustors. It was observed experimentally by Renaud *et al.* [4] using a similar combustor with the same injector designed for preheated liquid fuel. The flame of Renaud *et al.* was numerically reproduced in Large Eddy Simulations by Mesquita *et al.* [32,33], who explained the flame

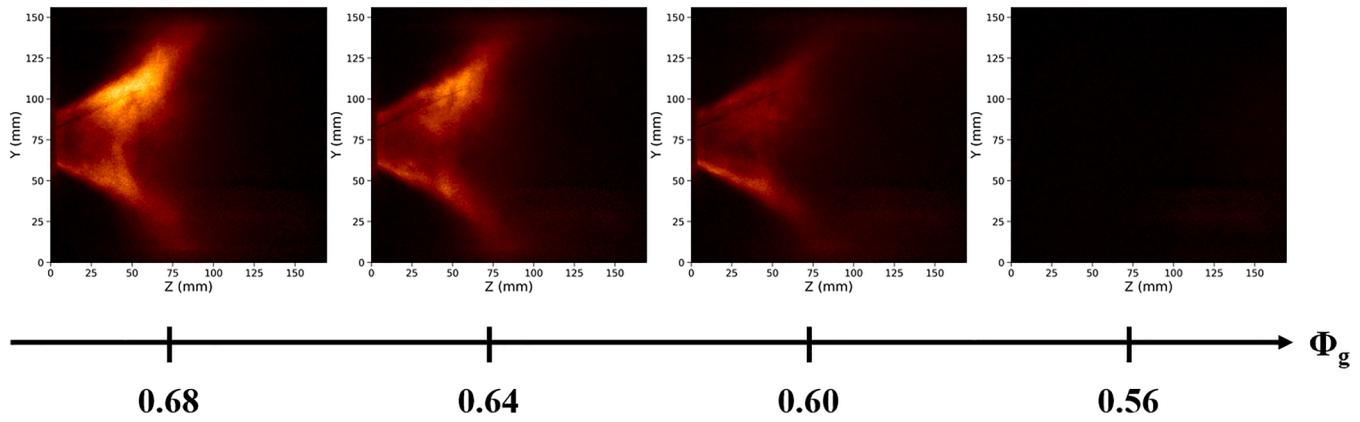


**Fig. 4.** CH* chemiluminescence average images of the LBO sequence of a 50-kW flame at α = 40% without NRP discharges

topology. Such calculations have not been performed so far in our gaseous case. Still, we assume that we can draw some conclusions on the flame topology from the knowledge of the liquid case simulations [33], which were initially carried out to study the flame dynamics with no link to plasma-assisted combustion.

Shear layers usually favor flame stabilization due to reduced flow velocity and enhanced mixing. The V-shape flame basis is anchored within the pilot stage and is stabilized over the Inner Shear Layer (ISL) delimiting the Central Recirculation Zone (CRZ) induced by the swirl motion of the flow. The CRZ of a V-shape flame is governed by a Conical Vortex Breakdown (CVB) mode [34,35], with the tip of the CRZ lying within the divergent nozzle of the injector. The CRZ radius increases linearly along the chamber axis, drawing the V-shape of the ISL and, thus, the shape of the flame. We see in Fig. 4 that the flame is not perfectly axisymmetric, possibly because the electrode creates recirculation patterns or a slight asymmetry of the injector. All experiments, with and without plasma, are performed with the electrode in place to solely investigate the NRP discharges effect.

The experiment is repeated under the same conditions but with NRP discharges applied at 33 kHz with an average deposited energy of 3.6 mJ. The images are shown in Fig. 5. The behavior down to $\Phi_g = 0.60$ is similar to the case without plasma. When the equivalence ratio is further decreased, the flame starts oscillating but blow-off does not occur. The flame is sustained through this unstable region between $\Phi_g = 0.56$ and $\Phi_g = 0.44$. This instability is characterized by the oscillation of the flame between the V shape and the tulip shape. When the equivalence ratio is further reduced, the flame again enters a stable regime, with a stable tulip-shape flame between $\Phi_g = 0.44$ and $\Phi_g = 0.38$. Once the flame is in the tulip shape, it gradually attenuates until blow-off.

The tulip-shape flame differs from the V-shape flame due to a CRZ resulting from a bubble vortex breakdown (BVB) mode [33]. In that case, the opening of the CRZ is less pronounced, it is bent and exhibits a constriction leading to its closing. It has the appearance of a tulip. The flame is anchored within the injector, and its branches are stabilized over the ISL. An interesting feature of the tulip-shape flame is its flow topology governed by a BVB mode similar to the cold flow, whereas the feedback of the V-flame on the flow leads to a CVB mode [33]. The common M-shape flame was not observed in this burner with gaseous methane. Like the tulip-shape flame, the M-shape flame is stabilized by a bubble CRZ, but the flame branches do not penetrate the injector nozzle.

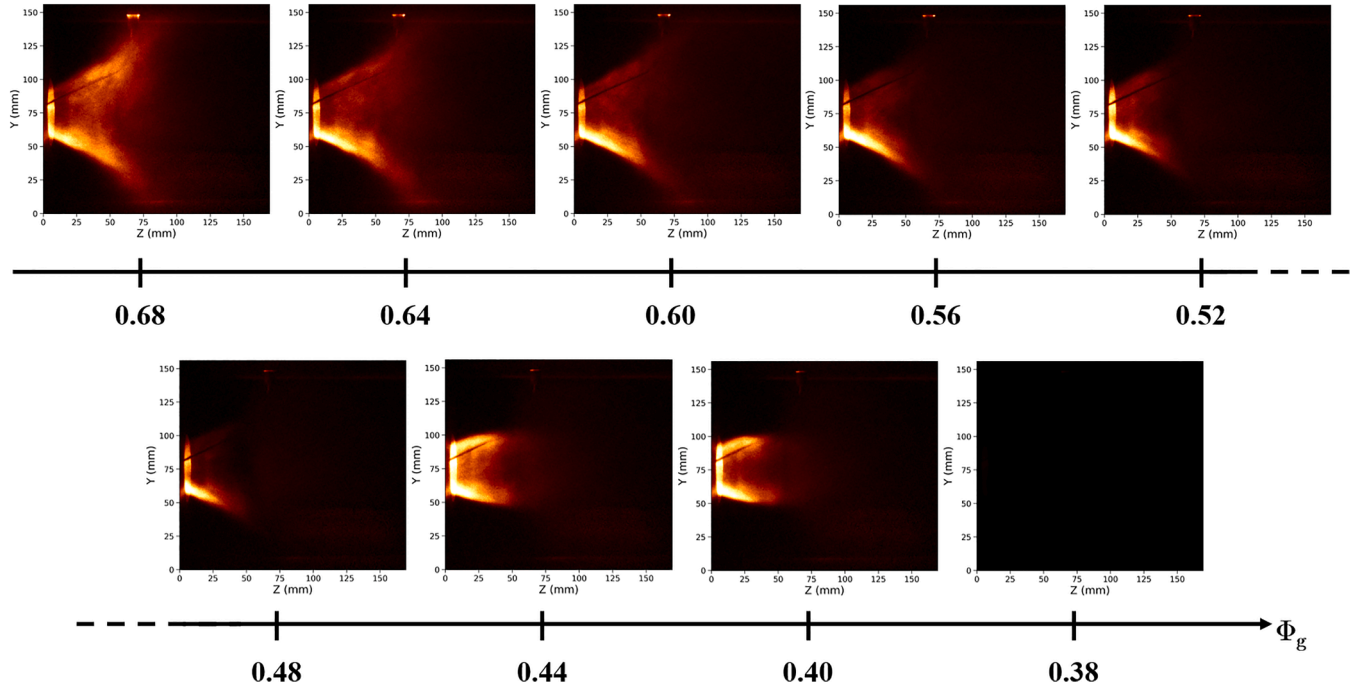


**Fig. 5.** CH* chemiluminescence average images of the LBO sequence of a 50-kW flame at α = 40% with 3.6-mJ NRP discharges applied at 33 kHz.

The leading edge of the M-shape flame is located at the end of the CRZ at the bottle-neck constriction where the bubble is closing (see [33] for full comparison of the three flame shapes in the liquid-fuel version of this burner). Likely, the M-shape does not exist when using gaseous methane in this burner, as the M-shape flame is highly dependent on spray dynamics and fuel droplet evaporation when using liquid fuel.

Starting from a V-shape flame and decreasing the equivalence ratio by increasing the air flow rate, the CVB mode transits to a BVB mode. Without plasma, this transition is responsible for flame extinction. However, when NRP discharges are applied, the combustion is maintained across the transition, and we obtain a stable tulip-shape flame until lean extinction. The change of flame shape is governed by the transition of the vortex breakdown mode. This shows that the NRP discharges are able to maintain the flame even when the flow is unstable in the rapid transition phase.

In Ref. [36], Terhaar *et al.* characterized the vortex breakdown induced by an injector composed of a central axial injection and a radial swirler. Their geometry is similar to the pilot stage of our injector except that they had the possibility to vary the geometrical swirl number thanks to movable vanes. They defined $\chi$ the axial injection fraction, corresponding to the ratio of the axial mass flowrate to the total mass flowrate injected in the chamber, and they performed a parametric study on the axial injection fraction and the geometrical swirl number. They observed that for a given swirl number, the transition from a CVB mode to a BVB mode occurs when the axial injection fraction decreases. In our case, knowing the global equivalence ratio $\Phi_g$, the fuel staging factor $\alpha$, and the stoichiometric methane-to-air mass ratio, denoted $\gamma_s$, we get:

$$\chi = \frac{\alpha \phi_g \gamma_s}{1 + \phi_g \gamma_s} \tag{4}$$

The axial injection fraction diminishes with the decreasing equivalence ratio. Thus, it could trigger the transition from the V-shape flame to the tulip-shape flame. Moreover, as the flame becomes leaner, its temperature diminishes as well. The feedback of the flame on the flow may not be sufficient to sustain the CVB mode as the BVB mode governs the cold flow topology. These two reasons possibly explain the flame shape transition when decreasing the equivalence ratio and require further investigations.

It is then legitimate to wonder whether the NRP discharges are helpful only to sustain the flame across the transition and whether the tulip-shape flame could exist without plasma. Turning off the NRP discharges once the flame is in the tulip shape leads to a non-immediate blow-off. However, this tulip-shape flame without NRP discharges has a short lifetime, from a few seconds up to a couple of minutes. Yet, it consistently extinguishes. The NRP discharges are thus crucial to prevent flame blow-off during the transition region and to stabilize the tulip-shape flame down to the LBO limit.

Furthermore, the evolution of the flame shape with the equivalence ratio does not exhibit a hysteresis cycle. Increasing the equivalence ratio from $\Phi_g = 0.40$ to $\Phi_g = 0.68$, we observe the same region of existence for the tulip-shape flame, the transition, and the V-shape flame as what we observe when decreasing the equivalence ratio from $\Phi_g = 0.68$ to $\Phi_g = 0.40$.

Flame-shape transitions in swirl-stabilized combustors were already observed by Kim *et al.* [21], Choe & Sun [25], and Vignat *et al.* [20]. Applying NRP discharges in a lean flame at steady conditions, Kim *et al.* observed a transition from a flame stabilized in the outer recirculation zone to a flame stabilized in the central recirculation zone. Choe & Sun found similar results at several flame thermal powers and equivalence ratios. For different flames that were not stabilized over the inner shear layer, they observed that applying NRP discharges begets the flame stabilization over the inner shear layer. Vignat *et al.* decreased the equivalence ratio of liquid n-heptane and dodecane flames. Without plasma, they observed that the flame becomes unstable and extinguishes, but by applying NRP discharges, they were able to sustain the flame in a shape that does not exist without plasma. The oscillation phase induced by the flame-shape transition was responsible for the flame extinction without plasma, as is the case in the present work.

### 3.2. Impact of fuel staging on LBO limit extension at 50 kW with NRP discharges

In this study, we are working at a constant flame thermal power. Leaner mixtures are obtained by increasing the air flowrate at constant fuel flowrate. Three distinct extinction mechanisms are encountered: V-shape flame blow-off, tulip-shape flame blow-off, and lifting of the V-shape flame, followed by the growth of the lift-off height until extinction. In the latter case, the lift-off height of the flame potentially extends to 40 cm, which means that there is still a burning region almost at the outlet of the combustion chamber. A typical example of a lifted flame is shown in Fig. 6. These lifted flames are not desired in practical applications because the combustion chamber should be as compact as possible, and because the flame lift-off height is not precisely controlled. Such flames were observed by Renaud *et al.* [4] and simulated by Mesquita *et al.* [37]. The lifted flame has a flow topology characterized by a CRZ resulting from a BVB mode. In that case, the flame is stabilized over the outer shear layer (OSL) and is not anchored within the injector. Mesquita *et al.* concluded that these flames are unsuitable for staged-injection combustors compared to other types of stabilized flames. In all the following experiments, the global equivalence ratio at blow-off, $\Phi_{LBO}$, is therefore defined as the equivalence ratio when the flame stops burning or stops being anchored within the injector. We thus consider lifted flames as blown off in this particular situation.

The LBO limit of 50-kW flames is investigated for fuel staging factors, α, varying from 0% to 100%. For each flame, the global equivalence ratio at blow-off, $\Phi_{LBO}$, is determined without and with plasma following the procedure described in Section 2.3. The results are presented in Fig. 7. A value of α = 0% corresponds to a methane injection through the multipoint stage only, and conversely, α = 100% corresponds to a methane injection through the pilot stage only. For instance, the equivalence ratio at LBO without plasma is 0.53 for the pilot-only flame and 0.93 for the multipoint-only flame. This difference is explained by the extinction mechanisms at stake in these two cases. For the pilot-only flame, the V-shape flame without plasma is blown off, whereas for the multipoint-only flame, $\Phi_{LBO} = 0.93$ corresponds to the transition from the V-shape flame to the lifted flame.

Without plasma (black squares), the LBO limit decreases with α. We

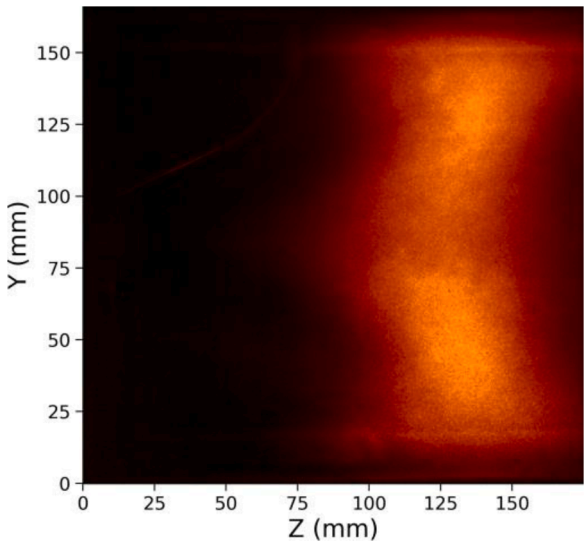


**Fig. 6.** CH* chemiluminescence average image of a lifted flame: 50 kW, α = 0%, $\Phi_g = 0.8$, without NRP discharges.

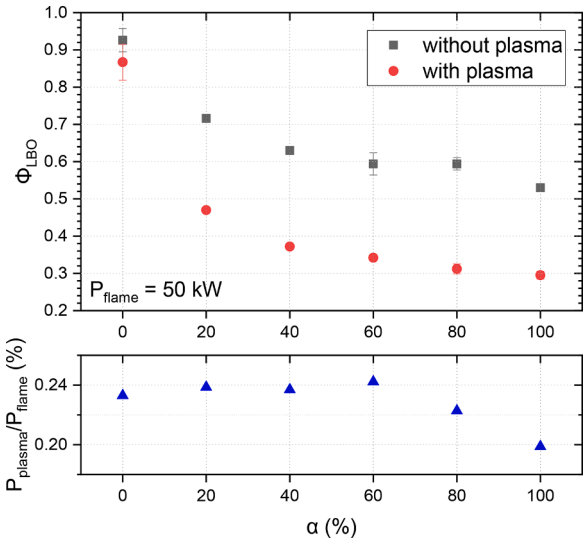


**Fig. 7.** (top) Lean blow-off limit of 50-kW flames without plasma (black squares) and with plasma (red circles) for fuel staging factors from 0% to 100%. (bottom) Plasma-to-flame power ratios. Error bars correspond to the standard deviation of the measurements. α = 0% corresponds to multipoint-only fuel injection and α = 100% corresponds to pilot-only fuel injection.

saw in Section 3.1 that, without plasma, the extinction is triggered by the transition from a CVB mode to a BVB mode governed by the value of $\chi$, the axial injection fraction. Eq. (4) shows that $\chi$ is proportional to α and decreases when $\Phi_g$ decreases. Thus, a V-shape flame of given equivalence ratio is closer to the critical value of $\chi$, determining the transition from the CVB to the BVB mode when the fuel staging factor is lower. This suggests that, decreasing the equivalence ratio, the flame will reach the LBO limit at a higher equivalence ratio for lower values of α. It could explain the better LBO performances for the highest values of α. This behavior is clearly observed in Fig. 7.

With plasma, the evolution of the equivalence ratio at LBO with the fuel staging is similar to the case without plasma: a greater value of α leads to a better extension of the LBO limit. Moreover, we note that with the NRP discharges, the domain of existence of the lean flames is dramatically extended. For α between 20% and 100%, $\Phi_{LBO}$ is divided by a factor of 1.5 to 1.9. Furthermore, for all values of α, the extinction sequences without and with plasma are similar to the case at α = 40% presented in Section 3.1. Without plasma, the V-shape flame blows off, whereas with plasma, there is a transition to the tulip-shape flame that blows off when the equivalence ratio is further reduced.

The evolution of the LBO performances with the fuel staging factor α with plasma is explained by the flow topology and more precisely, by the bubble vortex breakdown mode of the tulip-shape flame. Due to the dual injection system, a segregation of the flows coming from the two stages can be observed [33]. Indeed, the mixture injected through the pilot stage recirculates mainly in the CRZ close to the injector, whereas the flow coming from the multipoint stage is convected downstream by the annular swirling jet and poorly mixed with the pilot flow. For smaller values of the fuel staging α, the methane flow rate injected through the pilot stage is lower, and there is less methane approaching the CRZ to feed the flame; when the air flow rate is increased, the extinction occurs sooner. In other words, the local equivalence ratio in the burning region is closer to the pilot equivalence ratio (see Eq. (2)) than to the global equivalence and then more sensitive to fuel staging. For smaller values of α, the local equivalence ratio close to the burning region thus becomes smaller. Furthermore, due to this fuel segregation, the methane of the multipoint stage is convected far from the flame, barely approaches the CRZ to feed the burning region, and is presumably not entirely burnt, as detailed later in Section 4.1. For these reasons, the LBO extension is more challenging for small values of fuel staging with this injector and electrode geometry.

At α = 0%, the extension of $\Phi_{LBO}$ with plasma is less pronounced. The flame lift-off is slightly delayed, but the flame anchoring is not significantly improved as the equivalence ratio is further reduced. In this multipoint-only configuration, all the methane is injected through the multipoint stage, and only air is injected through the pilot stage. The flame without plasma is lifted (see Fig. 6). When the plasma is applied, the NRP discharges are located on the rim of the divergent portion of the pilot stage (see Fig. 2(a)), and we have seen that the flow of the pilot stage barely mixed with the flow of the multipoint stage. The reactive species and heat produced by the plasma in air [38,39] are thus inefficient because of their short lifetime and because they do not mix with the multipoint methane-air flow. To complete this aspect of the flow topology and the location of the discharges, one has to note that in the case α = 0%, the NRP discharges are applied in air only. In contrast, for higher values of α, they are applied in a methane-air mixture or in burnt gases. This could also partially explain their limited effectiveness. The electrode position should thus be changed to promote a more efficient interaction between the reactive species produced by the NRP discharges and the methane-air mixture of the multipoint stage; and in the end improve the stabilization of lean flames at α = 0%.

Finally, the plasma electric power is measured to evaluate the plasma-to-flame power ratio. For all experiments with plasma in this section, the NRP discharges are applied at a repetition frequency of 33 kHz. The discharge energy lies between 3 and 3.7 mJ, resulting in a plasma electric power between 100 and 120 W. Even without optimizing the repetition frequency or the energy deposited, less than 0.24% of the flame thermal power is sufficient to produce the plasma stabilizing the lean flames (Fig. 7-bottom).

### 3.3. LBO limit characterization from 20 kW to 100 kW

The gain in the LBO limit with NRP discharges for flame thermal powers from 20 kW to 100 kW is quantified and represented in Fig. 8.

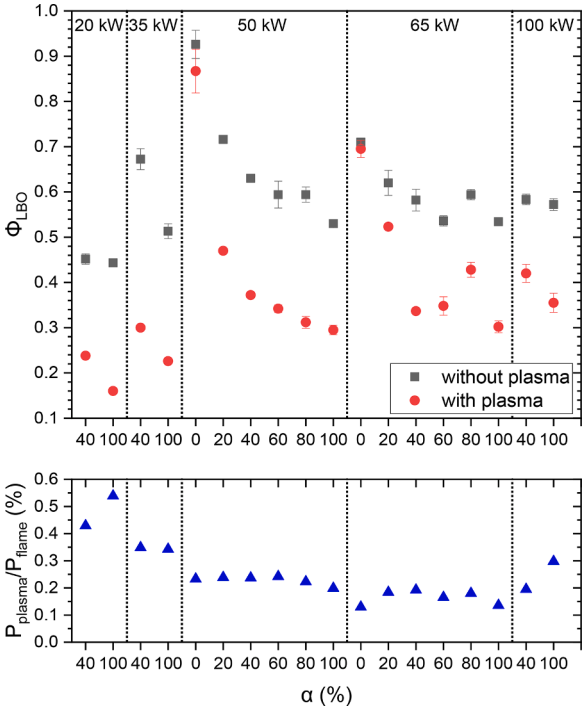


**Fig. 8.** (top) Stability map of the burner with and without NRP discharges for different fuel staging factors and flame thermal powers. (bottom) Plasma-to-flame power ratio. Error bars correspond to the standard deviation. α = 0% corresponds to multipoint-only fuel injection and α = 100% corresponds to pilot-only fuel injection.

**Table 1**
Summary of the operating conditions under consideration for the LBO extension.

| $P_{flame}$ (kW) | α (%) |
|---|---|
| 20 | 40-100 |
| 35 | 40-100 |
| 50 | 0-20-40-60-80-100 |
| 65 | 0-20-40-60-80-100 |
| 100 | 40-100 |

Table 1 summarises the operating conditions. Except at α = 0% for the reasons explained in Section 3.2, the LBO limit is drastically decreased with NRP discharges for all the investigated operating conditions and is divided by a factor of 2.8 in the best case and 1.2 in the less efficient case. Lean flames with plasma are stabilized at equivalence ratios below 0.5 and down to 0.16. Such low values were already obtained in swirl-stabilized combustors but at reduced flame thermal powers in Refs. [13,25]. We also observe that the NRP discharges produce better results in terms of LBO extension at higher fuel staging because of their location in the pilot stage of the injector. For all the fuel staging factors at every power investigated, the extinction mechanism is similar to the case presented in Section 3.1 (V-to-tulip transition), except for α = 0% at 50 kW and 65 kW where the flame is lifted. The benefit of NRP discharges to extend the operation range of this type of injector is hence evidenced.

At higher flame thermal powers, we had to apply the discharges at a higher repetition frequency, and thus higher plasma power, to maintain the flame across the V-to-tulip flame transition. Interestingly, depending on the fuel staging factor, the repetition frequency necessary to maintain the flame across the transition also varies. For a flame thermal power of 100 kW, discharges applied at 50 kHz are sufficient to stabilize the lean flame at α = 40%, but at α = 100% the frequency must be at least 77 kHz. This trend needs further investigation, but it indicates that the required plasma power decreases with the fuel staging factor, which is desirable as this injector is intended to operate with small values of α to achieve a premixed regime. For all values of α, the ratio of the plasma-to-flame power remains below 0.54%. At 100 kW, this ratio is further reduced to 0.19%. Recalling that we did not perform any energy optimization, these results are very promising for future practical applications. Finally, we see in Fig. 8 that the plasma-to-flame power ratio appears to decrease with increasing flame power. However, this trend is irrelevant considering that we kept the same peak voltage at 50 kW and 20 kW. Optimizing the plasma power, which is not the objective of this work, would undoubtedly have led to a lower plasma-to-flame power ratio for the less powerful flames than what we report.

A single experiment at 150 kW and α = 40% showed that the equivalence ratio at LBO can be extended from 0.56 without plasma to 0.42 with plasma. However, at such high power, we reach the safety limit of the facility. The measurements were not repeated and hence are not plotted in Fig. 8.

## 4. Combustion performance near blow-off

### 4.1. Combustion efficiency and pollutant emissions

For each fuel staging factor and flame thermal power, we plotted in Fig. 8 the equivalence ratio at blow-off without plasma and with plasma. To characterize the emissions of these flames near blow-off, we will operate at equivalence ratios slightly above the equivalence ratios at extinction. We denote $\Phi_{LBO\text{-}wo}$, the equivalence ratio 10% above the LBO without plasma, and $\Phi_{LBO\text{-}p}$, the equivalence ratio 10% above the LBO with plasma. At $\Phi_{LBO\text{-}wo}$ (V-shape flame), we characterize the emissions without plasma but also with plasma to investigate the effects of NRP discharges in these flames. At $\Phi_{LBO\text{-}p}$ (tulip-shape flame), we only characterize the emissions with NRP discharges because these flames do not exist without plasma.

Fig. 9 shows the combustion efficiency, $\eta_c$, and the mole fractions of $NO_X$, CO, and $N_2O$ ($N_2O$ is a greenhouse gas with a global warming potential 310 times larger than $CO_2$ [40]). For each fuel staging factor and flame thermal power, we represent the results at the equivalence ratio $\Phi_{LBO\text{-}wo}$ without plasma (black squares) and with NRP discharges (red circles) and also at the equivalence ratio $\Phi_{LBO\text{-}p}$ when NRP discharges are applied (blue triangles).

#### 4.1.1. Combustion efficiency

Fig. 9(a) shows that applying NRP discharges in the 20-kW flames significantly improves the combustion efficiency near blow-off. For higher flame thermal powers, the combustion efficiency of the V-shape flame at $\Phi_{LBO\text{-}wo}$ without discharges is already above 95%, but still increases slightly when NRP discharges are applied. The combustion efficiency of these flames near blow-off is high because during the extinction sequence, as the equivalence ratio is reduced, we do not observe a gradual attenuation of the flame. It means that, in this burner, high-power V-shape flames near blow-off have a very good combustion efficiency over the whole range of fuel staging factors.

At $\Phi_{LBO\text{-}p}$, the combustion efficiency of the tulip-shape flames considered in Fig. 9(a) (blue triangles) lies between 30% and 40% for the fuel staging factors between 40% and 100% and falls down to about 15%-20% at α = 20%. Decreasing the equivalence ratio, we observe a gradual attenuation of the tulip-shape flames (see Fig. 5). Although the combustion efficiency of the tulip-shape flames is less than that of the V-shape flames, they still release significant thermal power for low electric power. For instance, the 40% combustion efficiency of a 50-kW flame corresponds to a thermal power of 19 kW for a plasma power input of only 104 W (3.15±1.00 mJ per discharge at 33 kHz). For the 50-kW and 65-kW flames at α = 0%, we represent only the measurements without and with plasma at $\Phi_{LBO\text{-}wo}$ since LBO limits without and with plasma are very close (see Fig. 7).

According to the numerical simulations of a comparable two-stage injector [33], the tulip-shape flame exhibits a greater segregation of the flow coming from the two stages compared to the V-shape flame. This means that, in the tulip shape, the multipoint flow poorly mixes with the pilot flow which preferentially fills the central recirculation zone and thus the reaction zone. In other words, the flow coming from the multipoint stage is probably partially unburnt due to the flow topology that naturally prevents its mixing with the pilot flow and its penetration in the central recirculation zone. This is accentuated as the fuel staging factor is lowered, i.e., dominated by multipoint fuel.

#### 4.1.2. NOx emissions

Fig. 9(b) shows the $NO_X$ concentrations near blow-off with and without plasma. For the case without plasma, we observe that the $NO_X$ concentrations (black squares) increase with α, whereas the LBO limit decreases with α (see Fig. 8). This is particularly clear at 65 kW: for multipoint-only injection (α = 0%), $\Phi_{LBO\text{-}wo}$ = 0.71 and $X_{NOx}$ = 0 ppm (below detection limit), whereas for pilot-only injection (α = 100%), $\Phi_{LBO\text{-}wo}$ = 0.53 and $X_{NOx}$ = 6 ppm. This confirms that the multipoint strategy benefits $NO_X$ reductions, even though the multipoint-only flames blow off at a higher equivalence ratio than pilot-only flames.

Moreover, one of the objectives of plasma-assisted combustion is to stabilize lean flames in order to reduce $NO_X$ emissions. In Refs. [23,24], however, as the equivalence ratio was decreased, the level of $NO_X$ remained constant for flames stabilized with NRP discharges. In contrast, the present work shows that, for 75% of the flames investigated, the $NO_X$ concentrations in the leanest flames stabilized with NRP discharges (blue triangles) are lower than the $NO_X$ concentrations in the leanest stable flames without discharges (black squares) or are below the detection limit of the gas analyzer (see Fig. 9(b)). Thus the $NO_X$ concentrations are effectively reduced.

We know from previous studies that applying plasma in a flame tends to produce additional $NO_X$. This is confirmed in Fig. 9(b) for all flames investigated: at $\Phi_{LBO\text{-}wo}$, the $NO_X$ concentrations with plasma (red

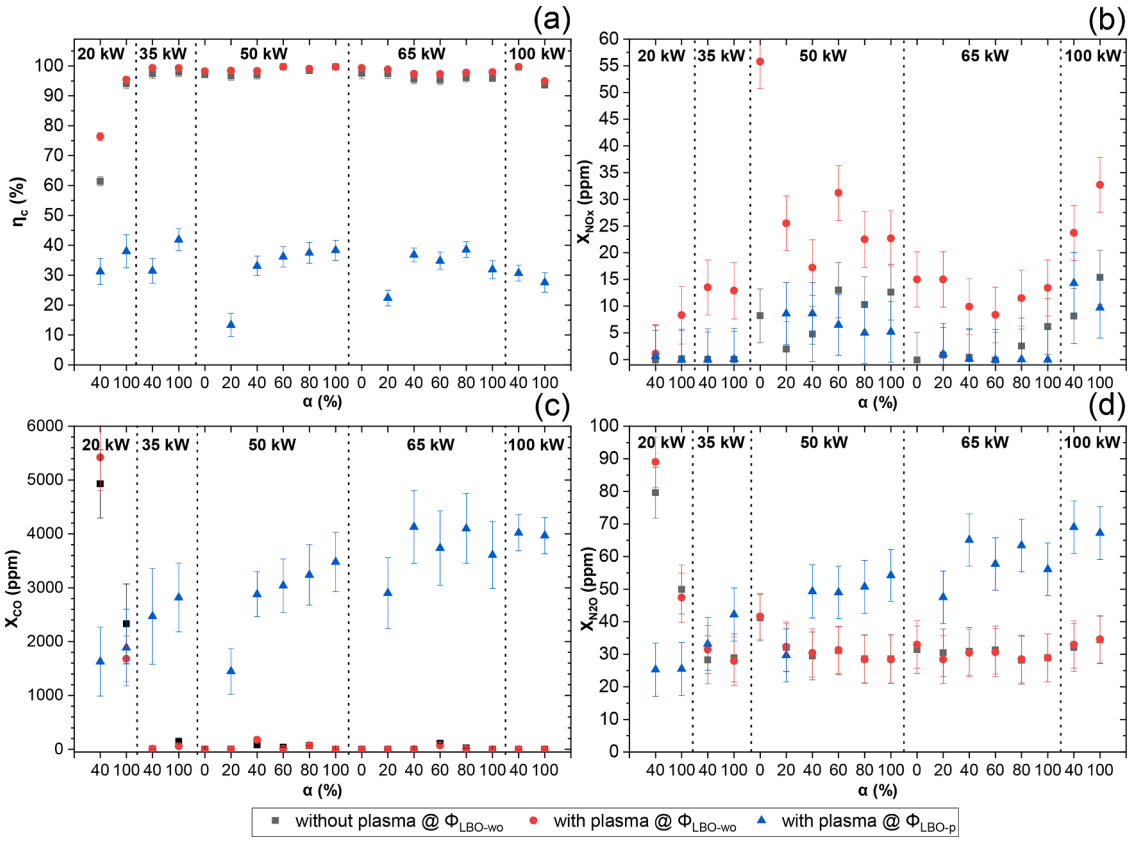


**Fig. 9.** Combustion efficiency (a) and mole fractions of $NO_X$ (b), CO (c), and $N_2O$ (d) near blow-off at the burner exit for different fuel staging factors of 20-kW to 100-kW flames, without plasma at $\Phi_{LBO\text{-}wo}$ (black squares), with plasma at $\Phi_{LBO\text{-}wo}$ (red circles), and with plasma at $\Phi_{LBO\text{-}p}$ (blue triangles). α = 0% corresponds to multipoint-only fuel injection and α = 100% corresponds to pilot-only fuel injection.

circles) are higher than without plasma (black squares). There are two sources of $NO_X$ production: the flame and the plasma. At $\Phi_{LBO\text{-}wo}$, if we assume that the slight improvement of the combustion efficiency with plasma (see Fig. 9(a)) is not sufficient to explain the increase of $NO_X$ concentrations, we can deduce the contribution of the plasma to the overall $NO_X$ concentration by subtracting the $NO_X$ concentration of the non-assisted flame (black squares) to the $NO_X$ concentration of the assisted flame (red circles). For instance, at $\Phi_{LBO\text{-}wo}$ we measure 13±5 ppm in the non-assisted 50-kW flame at α = 100% and 23±5 ppm in the assisted flame. We deduce that 10±7 ppm are produced by the plasma.

To further investigate the production of $NO_X$ by lean plasma-assisted flames, Fig. 10 plots the flame contribution to $NO_X$ concentrations at $\Phi_{LBO\text{-}wo}$ (black bars), the plasma contribution to $NO_X$ concentrations at $\Phi_{LBO\text{-}wo}$ (red bars, obtained by subtracting black square values to red circle values), and the $NO_X$ concentrations of the assisted flames at $\Phi_{LBO\text{-}p}$ (blue bars). Blue bars are always smaller than red bars, in other words the $NO_X$ concentrations of the assisted flames at $\Phi_{LBO\text{-}p}$ are lower than the plasma contribution to $NO_X$ concentrations at $\Phi_{LBO\text{-}wo}$. This is only due to the reduction of equivalence ratio because the average plasma power remains unchanged as shown in Fig. 11. Therefore, when reducing the equivalence ratio at constant plasma power, both the flame and the plasma contribution to $NO_X$ concentration are decreased. This latter observation is consistent with the work of Lacoste *et al.* [24], who showed that $NO_X$ concentrations increase linearly with the plasma power per unit mass of air injected in their combustor. In the present work, we reduce the equivalence ratio by increasing the air flow rate. Therefore, when reducing the equivalence ratio at constant power, the $NO_X$ produced by the flame are reduced, as expected, but in addition the $NO_X$ produced by the plasma itself are also reduced. Thus, the additional $NO_X$ produced by the plasma can be partially mitigated.

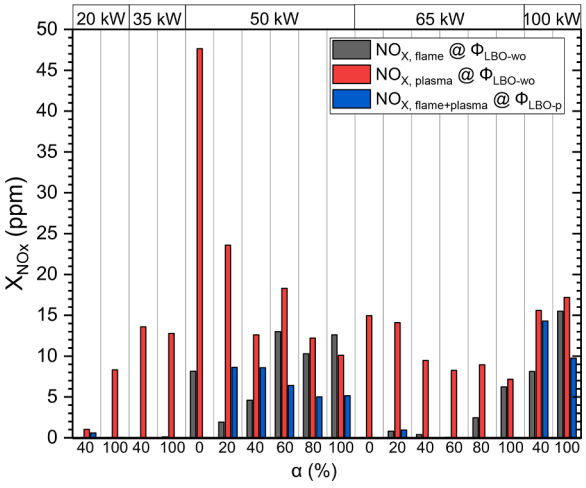


**Fig. 10.** Flame contribution to $NO_X$ concentrations at $\Phi_{LBO\text{-}wo}$ (black bars), plasma contribution to $NO_X$ concentrations at $\Phi_{LBO\text{-}wo}$ (red bars), and $NO_X$ concentrations of the assisted flames at $\Phi_{LBO\text{-}p}$ (blue bars) for all conditions investigated.

### 4.1.3. *CO and $N_2O$ emissions*

As shown in Fig. 9(c) and (d), the concentrations of CO and $N_2O$ of the V-shape flames at $\Phi_{LBO\text{-}wo}$ are reduced for the 20-kW flames when NRP discharges are applied, which is certainly due to the combustion efficiency improvement. For higher flame thermal powers, the CO and $N_2O$ concentrations do not change by applying NRP discharges for any fuel staging factors or flames. However, the tulip-shape flame with NRP

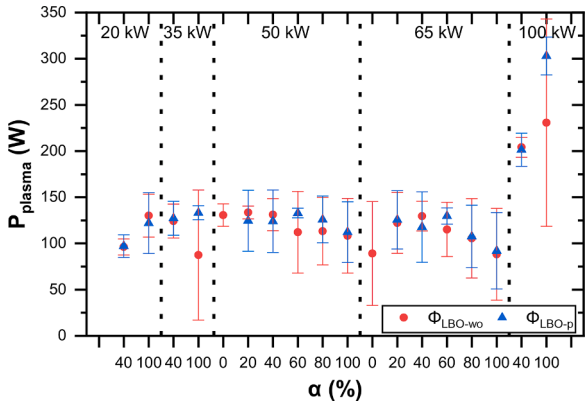


**Fig. 11.** Average plasma power at $\Phi_{LBO\text{-}wo}$ (red circles) and $\Phi_{LBO\text{-}p}$ (blue triangles). Error bars correspond to the standard deviation of the measurements.

discharges at $\Phi_{LBO\text{-}p}$ (blue triangles) produces a level of CO and $N_2O$ greater than the V-shape flame with NRP discharges (red circles) for almost all fuel staging factors and flame thermal powers. This can be explained once again by the flow topology. The bubble vortex breakdown mode of the central recirculation zone is responsible for a poor mixing of the flow coming from the two stages. Thus, the tulip-shape flame is more prone to fuel-rich pockets of gas than an efficient fuel-air mixing [33]. This behavior was expected in [33] to be responsible for higher pollutant emissions and is experimentally confirmed here. We also note that the concentrations of CO and $N_2O$ diminish at lower fuel staging factors, similar to the combustion efficiency. Still, this could also be attributed to an improved fuel-air mixing as more fuel is fed through the multipoint stage. In the following section, we will seek to determine whether the emissions of the tulip-shape flame are due to the discharges or to the flame itself.

### *4.2. Impact of NRP discharges on the combustion performances of a lean tulip-shape flame*

In most cases, the tulip-shape flame extinguishes rapidly when the NRP discharges are turned off. However, for a 50-kW flame at $\alpha = 80\%$ and $\Phi_g = 0.37$, the tulip-shape flame survives long enough (more than 2 minutes) to perform measurements of the exhaust gas composition without plasma. We can thus compare the combustion efficiency and the $NO_X$, CO, and $N_2O$ emissions of a tulip-shape flame without and with NRP discharges applied at 33 kHz. The results are shown in Fig. 12. We observe that without plasma the $N_2O$ and CO emissions of the flame are already high, and applying the discharges alters only slightly these emissions. Regarding the $NO_X$ emissions, without plasma they are below the detection limit, and with plasma they remain very low (less than 2 ppm).

Based on this comparison, we conclude that the high levels of CO and $N_2O$ emissions of the tulip-shape flame with NRP discharges can be attributed to the flame itself (and its particular tulip topology) rather than the discharges. NRP discharges are even beneficial to increase the combustion efficiency.

## 5. Effect of pulsing patterns on the stability and combustion performance of a lean flame stabilized by NRP discharges

In this section, instead of applying NRP discharges continuously, we apply the discharges in a duty cycle mode in order to tailor the energy distribution. The pulse pattern, illustrated in Fig. 13, consists first of a burst containing $N_{ON}$ discharges applied at a repetition frequency $f_R$. Then, we wait for a number of periods (the duration of a period being defined as $\tau_R = 1/f_R$), denoted $N_{OFF}$, before applying the next burst of discharges. The duty cycle ratio, $r_{DC}$, is the ratio of the duration of the burst of NRP discharges to the duration of the pattern:

$$r_{DC} = \frac{N_{ON}}{N_{ON} + N_{OFF}} \tag{5}$$

To modulate the pulse pattern, we maintain the pulse repetition frequency constant at 33 kHz, but we change $N_{ON}$ and $N_{OFF}$ to study: i) the impact of the cumulative effects of the discharges within a burst (via $N_{ON}$) and ii) the impact of the burst-to-burst coupling (via $N_{OFF}$). In the rest of this section, we operate with a 50-kW flame at $\alpha = 40\%$ and $\Phi_g = \Phi_{LBO\text{-}p} = 0.44$. It corresponds to a tulip-shape flame that does not exist without plasma (see Fig. 8).

### *5.1. Stability map*

Applying various pulse patterns in the fresh mixture, we observe the three regimes depicted in Fig. 14(a). The "stabilized flame" is observed when the applied pulse pattern ignites the flame and ensures continuous combustion. The "intermittent flame" corresponds to a flame that remains stable for a few hundred bursts (i.e., a few seconds) but is then blown off before being reignited and stabilized for a few seconds so that the cycle is repeated. This cannot be considered as a succession of ignition events because we do not observe a flame extinction between each burst. Still, the applied pulse pattern does not ensure continuous combustion. The third regime is the "no flame" case when there is no ignition at all. When the discharges are applied continuously, the flame is stable. Therefore, for $r_{DC}$ close to 1, the flame is stabilized for any value of $N_{ON}$. When $r_{DC}$ is decreased, the flame eventually either extinguishes (for short bursts with $N_{ON} < 100$) or becomes intermittent

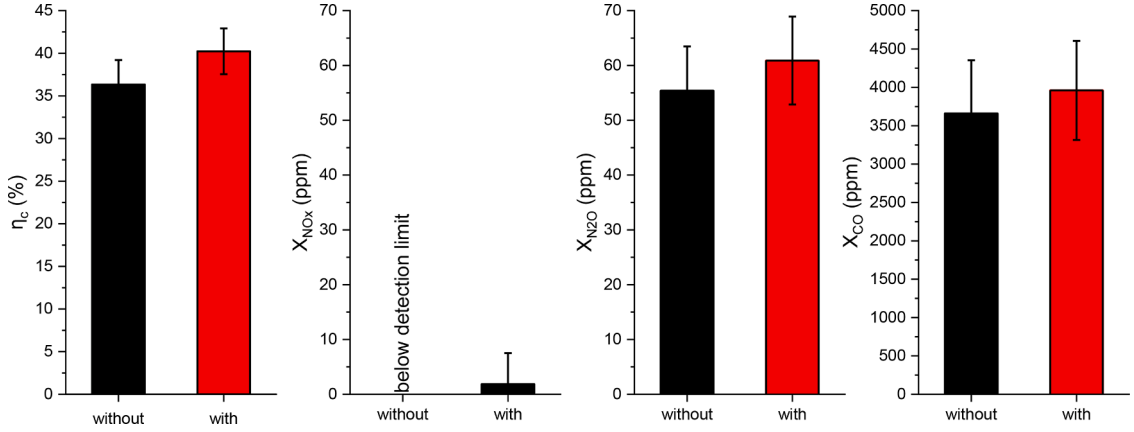


**Fig. 12.** Comparison of the combustion efficiency and emissions without and with NRP discharges applied at 33 kHz with an average deposited energy of 3.4±0.8 mJ in a 50-kW tulip-shape flame at $\alpha = 80\%$ and $\Phi_g = 0.37$.

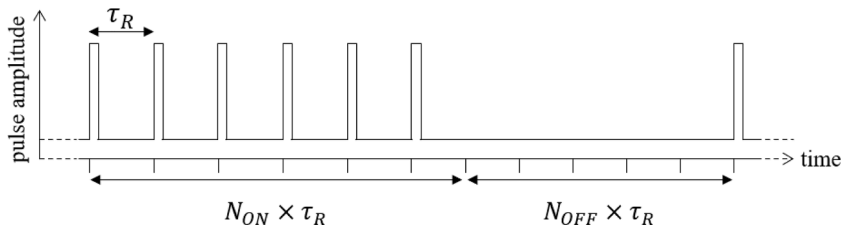


**Fig. 13.** Timing diagram of NRP discharges applied in a duty cycle mode at a repetition frequency $f_R$ with $\tau_R = 1/f_R$. In this example, $N_{ON} = 6$ and $N_{OFF} = 5$.

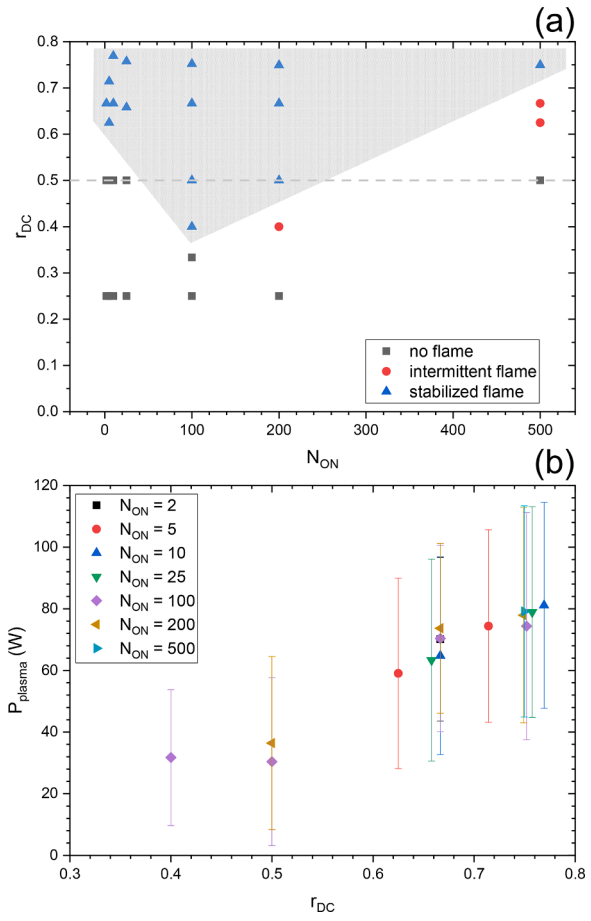


**Fig. 14.** (a) Stability domain of the flame (50 kW, $\Phi_g = 0.44$, $\alpha = 40\%$) depending on the number of pulses in the burst ($N_{ON}$) and the duty cycle ratio ($r_{DC}$) and (b) average plasma power for the pulse patterns permitting a "stabilized flame".

(when $N_{ON} > 100$).

For long bursts ($N_{ON} > 100$), there are enough discharges within each burst for the cumulative effect of the discharges to create an ignition kernel that further propagates. Stabilization is achieved when the coupling between consecutive bursts (burst-to-burst coupling) is strong. When $r_{DC}$ decreases, the flame eventually becomes intermittent. There is still some burst-to-burst coupling because the flame burns for a few seconds (hundreds of bursts) between two extinctions. However, this coupling is at the limit to fully sustain the combustion of this turbulent flame.

For short bursts ($N_{ON} < 100$), when reducing $r_{DC}$, we do not observe intermittent flames: the cumulative effects of the discharges within one burst are not sufficient to produce an ignition kernel, and $N_{OFF}$ is too important to produce an ignition kernel thanks to the burst-to-burst coupling. For example, if $N_{ON} = 5$, even for $r_{DC} = 0.5$, no ignition or flame stabilization occurs because 5 discharges are not sufficient to generate an ignition kernel in this experiment. Thus, for short bursts, the flame can only be stabilized thanks to burst-to-burst coupling when $N_{OFF}$ is sufficiently low. The dynamics are then closer to the case of discharges applied continuously.

In this experiment, the lowest $r_{DC}$ that ensures flame stabilization corresponds to $N_{ON} = 100$, which appears to be close to the minimum number of discharges necessary to ignite the mixture in this configuration. The stabilization ability of the pulse pattern thus depends on two effects: the cumulative effects of the discharges within each burst and the burst-to-burst coupling. The number of discharges in the burst must be sufficient to ensure a significant effect as a result of the cumulative effects of the discharges, and $r_{DC}$ can be reduced until the limit of efficient burst-to-burst coupling. The cumulative effects of the discharges have already been observed with a burst of discharges in air [41] or in a flame [42–44], if the repetition frequency is sufficiently high. They are due to a remanent heating and species production from the previous discharge in the interelectrode gap because the gas is not entirely renewed. During the first discharges, the temperature and concentration of radicals increase stepwise from discharge to discharge. Then, temperature and species concentration are balanced out by the gas motion and reach steady state. The duration of the transient regime (i.e. the number of discharges before reaching steady state) and the plateauing value for the temperature and species concentration depend on the repetition frequency. Adams *et al.* [41] investigated this inter-pulse coupling in air by applying a burst of 10 discharges at repetition frequencies from 1 to 250 kHz. They showed that, in their configuration, the cumulative effects became significant for repetition frequencies higher than 15 kHz. They also measured that the heating rate and the plateauing value of the temperature during the burst increased with the repetition frequency. Applying NRP spark discharges at 20 kHz in a lean premixed methane-air flame, Blanchard *et al.* [42], Bechane [43], and Minesi [44] showed experimentally and numerically that the temperature and the OH concentration built up during the first 10 discharges and then reached a plateau. In a stagnation plate burner, Del Cont-Bernard *et al.* [45] applied NRP glow discharges and also observed a stepwise increase of the OH LIF signal and then a steady state after thousands of discharges (due to the very low energy deposited by the NRP glow discharges).

Moreover, the burst-to-burst coupling was investigated by Dunn *et al.* [46] for ignition studies of lean methane-air flames using NRP discharges. They applied 10 discharges either in a continuous mode, i.e., at a given repetition frequency (between 2.5 and 10 kHz) or separated in packets of 2 or 3 discharges (with a delay of 3.3 to 33 µs between two consecutive discharges within a packet) but always holding the duration of the series of 10 discharges constant. They showed that the packet-to-packet interaction, or the burst-to-burst coupling, can be beneficial or detrimental to the ignition kernel but exhibits different dynamics than the constant repetition frequency regime. The burst-to-burst coupling also results from the remanent heating and species concentration of the previous burst.

Thus, depending on the pulse patterns, we expect different dynamics for the transient regime and the steady state within a burst (note that the steady state will be reached only if $N_{ON}$ is sufficiently large). For example, if $N_{OFF}$ is small, the burst-to-burst separation is too low for the gas to be renewed in the discharge volume, and the behavior will be

similar to what occurs when the discharges are applied continuously. However, if the burst-to-burst separation is sufficiently high, the gas is renewed in the discharge volume between consecutive bursts. We can then expect the thermal and chemical effects to be different from a regime of discharges applied continuously. The stability domain of the flame (see Fig. 14) illustrates the impact on flame stabilization of the cumulative effects within a burst and of the burst-to-burst coupling. The impact of the two effects on $NO_X$ emission is investigated in the next section.

Fig. 14(b) shows the average plasma power of all pulse patterns that enable flame stabilization in the present work. The average plasma power is defined as the average energy deposited by a discharge multiplied by the duty cycle ratio and the discharge repetition frequency (held constant at 33 kHz here): $P_{plasma} = r_{DC} \times E \times f_R$. For the pulse patterns tested, the plasma power varies linearly with the duty cycle ratio and does not depend on the number of discharges within each burst. For the lowest duty cycle ratio, the plasma power is 32 W against 116 W when the discharges are applied continuously (see Fig. 8). This represents a gain by a factor of 3.6 to stabilize the same flame. The minimal plasma-to-flame power ratio necessary to stabilize this flame is thus 0.06%.

### 5.2. $NO_X$ emissions

Fig. 15(a) shows the $NO_X$ concentration at the combustor exit plane as a function of the duty cycle ratio. The level of $NO_X$ is found to vary linearly with the duty cycle ratio. When $r_{DC}$ is decreased from 0.8 to 0.4, the $NO_X$ concentration is divided by a factor of 1.7. Knowing that the plasma power also varies linearly with $r_{DC}$ (see Fig. 14(b)), the $NO_X$ concentration increases linearly with the plasma power, as shown in Fig. 15(b). A similar variation of $NO_X$ with plasma power was observed in Refs. [15,21,24,25], but in these works, the authors varied the discharge repetition frequency or the deposited energy (via the peak voltage). Interestingly, the present work corroborates their conclusion on the $NO_X$ emissions increase with the plasma power even though, in our case, the discharges are not applied continuously but using various pulse patterns.

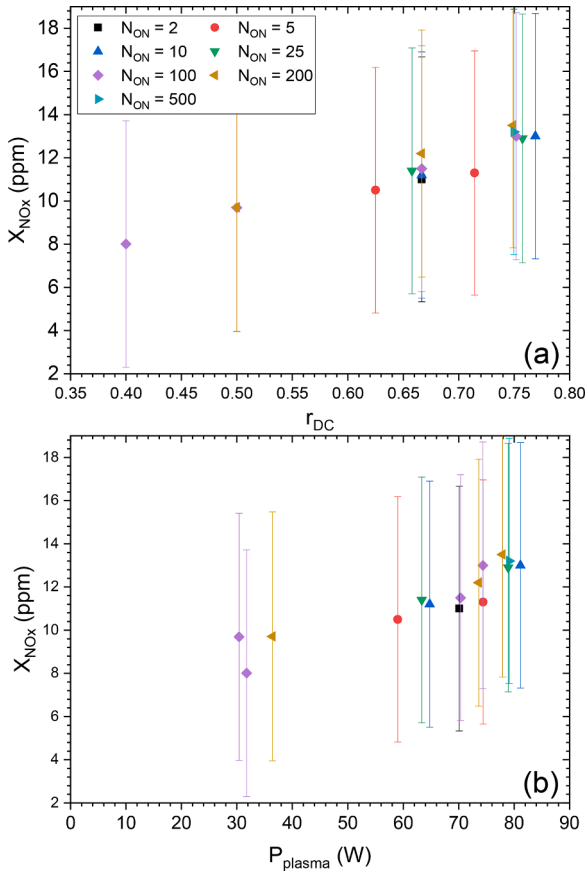


**Fig. 15.** Evolution of the $NO_X$ concentration at the chamber outlet for various pulse patterns of NRP discharges applied in a 50-kW flame at $\Phi_g = 0.44$ and $\alpha = 40\%$ as a function of (a) the duty cycle ratio and (b) the average plasma electric power.

For the range of discharge repetition frequencies, peak voltages, and pulse patterns studied in Refs. [15,21,24,25] and in the present work, the formation of $NO_X$ by NRP discharges is thus mainly governed by the average plasma power. For a given duty cycle ratio, the number of discharges within a burst does not seem to significantly affect $NO_X$ emissions, even though we could expect different thermal and chemical effects for the different pulse patterns. Additional studies with a broader range of duty cycle ratios, repetition frequencies (held constant in this work), and peak voltages would be helpful to investigate further the impact on $NO_X$ emissions of the cumulative effects within a burst and of burst-to-burst coupling.

## 6. Conclusions

This study shows that NRP discharges can effectively widen the operating range and improve the performances of gas turbines and aircraft engines. This work is novel in that it demonstrates the stabilization of lean flames in a gas turbine model combustor with a realistic injector composed of two stages of fuel injection: a pilot stage and a multipoint stage. The lean blow-off limit of swirl-stabilized flames is extended for flame thermal powers up to 100 kW for a wide range of fuel staging factors. The 100-kW flame is stabilized by NRP discharges down to an equivalence ratio of 0.35 (versus typically 0.6 without plasma), with a plasma-to-flame power ratio of only 0.19%. At the lean blow-out limit with plasma, the flame takes a tulip shape, which is shown to be governed by the flow topology. The tulip-shape flame stabilized with the discharges has a combustion efficiency of about 40%. This low combustion efficiency is probably due to the flow topology, which prevents part of the mixture coming from the multipoint stage from burning. We believe that better efficiency can be achieved by modifying the injector geometry to obtain a conical recirculation zone, thus stabilizing a lean V-shape flame instead of a tulip-shape flame. The tulip-shape flame is also found to emit less $NO_X$ than the leanest stable flames without plasma in 75% of the cases investigated. This important result contrasts with previous studies in which the plasma-stabilized flames always emitted more NOx than the leanest stable flames without plasma. The CO and $N_2O$ emissions are relatively high compared to richer V-shape flames stabilized without plasma. These higher emissions are explained by a detrimental fuel-air mixing induced by this particular flame shape and not by the plasma. Finally, we have shown that tailoring the energy deposition by applying the NRP discharges in a duty cycle mode significantly reduces the plasma power needed to stabilize lean flames (down to 0.06% of the flame thermal power) and further decreases the $NO_X$ concentrations at the burner exit. The cumulative effects within a burst and the burst-to-burst coupling are found to play a major role in the ability of a pulse pattern to stabilize lean flames. Moreover, it is found that $NO_X$ emissions decrease linearly with the average plasma power of the pulse patterns. However, more investigations are required to understand the impact of the pulse pattern on $NO_X$ chemistry, particularly the cumulative effects within a burst and the burst-to-burst coupling. Tailoring the pulse pattern enables to add flexibility in practical applications. For example, in aircraft propulsion, different pulse patterns optimized for LBO, $NO_X$ reduction, or CO reduction, can be used in various phases of flight.

## Declaration of Competing Interest

The authors declare that they have no known competing financial interests or personal relationships that could have appeared to influence the work reported in this paper.

## Acknowledgments

This work has received funding from the Agence Nationale de la Recherche (grant PASTEC ANR16-CE22-0005) and the European Research Council (ERC) under the European Union's Horizon 2020 research and innovation program (grant agreement No.101021538). A CC-BY 4.0 public copyright license has been applied by the authors to the present document and will be applied to all subsequent versions up to the Author Accepted Manuscript arising from this submission, in accordance with the grant's open access conditions: https://creativecommons.org/licenses/by/4.0/. The authors would like to thank Erika Jean-Bart, Yannick Le Teno, Hubert Jubeau, and Koro Sokhona for technical assistance with the experimental facility, Guilhem Lavabre for discussions on uncertainty quantification, and Renaud Gablier for discussions on $NO_X$ emissions.

## References

[1] Huang Y, Yang V. Dynamics and stability of lean-premixed swirl-stabilized combustion. Prog. Energy Combust. Sci. 2009;35:293–364. https://doi.org/10.1016/j.pecs.2009.01.002.
[2] Broda JC, Seo S, Santoro RJ, Shirhattikar G, Yang V. An experimental study of combustion dynamics of a premixed swirl injector. Symp. Combust. 1998;27:1849–56. https://doi.org/10.1016/S0082-0784(98)80027-1.
[3] Barbosa S, Scouflaire P, Ducruix S. Time resolved flowfield, flame structure and acoustic characterization of a staged multi-injection burner. In: Proc. Combust. Inst. 32 II; 2009. p. 2965–72. https://doi.org/10.1016/j.proci.2008.06.139.
[4] Renaud A, Ducruix S, Scouflaire P, Zimmer L. Flame shape transition in a swirl stabilised liquid fueled burner. Proc. Combust. Inst. 2015;35:3365–72. https://doi.org/10.1016/j.proci.2014.07.012.
[5] Lee JG, Kim K, Santavicca DA. Effect of injection location on the effectiveness of an active control system using secondary fuel injection. Proc. Combust. Inst. 2000;28:739–46. https://doi.org/10.1016/S0082-0784(00)80276-3.
[6] Hong B-S, Ray A, Yang V. Wide-range robust control of combustion instability. Combust. Flame. 2002;128:242–58. https://doi.org/10.1016/S0010-2180(01)00349-2.
[7] Choi G-M, Tanahashi M, Miyauchi T. Control of oscillating combustion and noise based on local flame structure. Proc. Combust. Inst. 2005;30:1807–14. https://doi.org/10.1016/j.proci.2004.08.249.
[8] Starikovskiy A, Aleksandrov N. Plasma-assisted ignition and combustion. Prog. Energy Combust. Sci. 2013;39:61–110. https://doi.org/10.1016/j.pecs.2012.05.003.
[9] Ju Y, Sun W. Plasma assisted combustion: Dynamics and chemistry. Prog. Energy Combust. Sci. 2015;48:21–83. https://doi.org/10.1016/j.pecs.2014.12.002.
[10] Pai DZ, Lacoste DA, Laux CO. Nanosecond repetitively pulsed discharges in air at atmospheric pressure-the spark regime. Plasma Sources Sci. Technol. 2010;19:065015. https://doi.org/10.1088/0963-0252/19/6/065015.
[11] Starikovskaia SM. Plasma-assisted ignition and combustion: nanosecond discharges and development of kinetic mechanisms. J. Phys. D. Appl. Phys. 2014;47:353001. https://doi.org/10.1088/0022-3727/47/35/353001.
[12] Laux CO. Applications of Plasma Discharges to Combustion. J. Combust. Soc. Japan. 2022;64:257–64. https://doi.org/10.20619/jcombsj.64.209_257.
[13] Barbosa S, Pilla G, Lacoste DA, Scouflaire P, Ducruix S, Laux CO, Veynante D. Influence of nanosecond repetitively pulsed discharges on the stability of a swirled propane/air burner representative of an aeronautical combustor. Philos. Trans. R. Soc. A Math. Phys. Eng. Sci. 2015;373:20140335. https://doi.org/10.1098/rsta.2014.0335.
[14] Blanchard VP, Roqué F, Scouflaire P, Laux CO, Ducruix S. Stabilization of lean flames with nanosecond discharges in a gas turbine model combustor. AIAA SciTech Forum 2023;2023:2023–387. https://doi.org/10.2514/6.2023-2387.
[15] Xiong Y, Schulz O, Bourquard C, Weilenmann M, Noiray N. Plasma enhanced auto-ignition in a sequential combustor. Proc. Combust. Inst. 2019;37:5587–94. https://doi.org/10.1016/j.proci.2018.08.031.
[16] Lacoste DA, Moeck JP, Durox D, Laux CO, Schuller T. Effect of Nanosecond Repetitively Pulsed Discharges on the Dynamics of a Swirl-Stabilized Lean Premixed Flame. J. Eng. Gas Turbines Power. 2013;135. https://doi.org/10.1115/1.4024961.
[17] Moeck JP, Lacoste DA, Laux CO, Paschereit CO. Control of combustion dynamics in a swirl-stabilized combustor with nanosecond repetitively pulsed discharges. In: 51st AIAA Aerosp. Sci. Meet. Incl. New Horizons Forum Aerosp. Expo. 2013; 2013. https://doi.org/10.2514/6.2013-565. 2013–0565.
[18] Shanbhogue SJ, Pavan CA, Weibel DE, Gomez del Campo F, Guerra-Garcia C, Ghoniem AF. Control of Large-Amplitude Combustion Oscillations Using Nanosecond Repetitively Pulsed Plasmas. J. Propuls. Power. 2023:1–13. https://doi.org/10.2514/1.B38883.
[19] Di Sabatino F, Lacoste DA. Enhancement of the lean stability and blow-off limits of methane-air swirl flames at elevated pressures by nanosecond repetitively pulsed discharges. J. Phys. D. Appl. Phys. 2020;53:355201. https://doi.org/10.1088/1361-6463/ab8f54.
[20] Vignat G, Minesi N, Soundararajan PR, Durox D, Renaud A, Blanchard V, Laux CO, Candel S. Improvement of lean blow out performance of spray and premixed swirled flames using nanosecond repetitively pulsed discharges. Proc. Combust. Inst. 2021;38:6559–66. https://doi.org/10.1016/j.proci.2020.06.136.
[21] Kim W, Snyder J, Cohen J. Plasma assisted combustor dynamics control. Proc. Combust. Inst. 2015;35:3479–86. https://doi.org/10.1016/j.proci.2014.08.025.
[22] Kim W, Do H, Mungal M, Cappelli M. Flame Stabilization Enhancement and NOx Production using Ultra Short Repetitively Pulsed Plasma Discharges. In: 44th AIAA Aerosp. Sci. Meet. Exhib.; 2006. p. 6770–2. https://doi.org/10.2514/6.2006-560.
[23] Stancu GD, Simeni MS, Laux CO. Investigations by Mid-IR QCLAS of pollutant emissions in high temperature exhaust gases released from plasma-assisted combustion. In: 31st ICPIG, July 14-19, 2013, Granada, Spain; 2013. p. 8–11.
[24] Lacoste DA, Moeck JP, Paschereit CO, Laux CO. Effect of Plasma Discharges on Nitric Oxide Emissions in a Premixed Flame. J. Propuls. Power. 2013;29:748–51. https://doi.org/10.2514/1.B34819.
[25] Choe J, Sun W. Blowoff hysteresis, flame morphology and the effect of plasma in a swirling flow. J. Phys. D. Appl. Phys. 2018;51:365201. https://doi.org/10.1088/1361-6463/aad4dc.
[26] Barbosa S. Étude Expérimentale De La Dynamique De Combustion D'Un Injecteur Multipoint Étagé De Turbine À Gaz. Ph.D. Thesis dissertation. Ecole Centrale Paris; 2008.
[27] Providakis T. Etude de la dynamique de flamme swirlée dans un injecteur diphasique multipoints étagé. Ph.D. Thesis dissertation. Ecole Centrale Paris; 2013.
[28] Renaud A. High-speed diagnostics for the study of flame stabilization and transient behaviour in a swirled burner with variable liquid-fuel distribution. Ph.D. Thesis dissertation. Ecole Centrale Paris; 2016.
[29] Minesi N, Stepanyan S, Mariotto P, Stancu G-D, Laux CO. Fully ionized nanosecond discharges in air: the thermal spark. Plasma Sources Sci. Technol. 2020;29:85003. https://doi.org/10.1088/1361-6595/ab94d3.
[30] Minesi NQ, Blanchard VP, Pannier E, Stancu GD, Laux CO. Plasma-assisted combustion with nanosecond discharges. I: Discharge effects characterization in the burnt gases of a lean flame. Plasma Sources Sci. Technol. 2022;31:045029. https://doi.org/10.1088/1361-6595/ac5cd4.
[31] Blanchard VP, Roque F, Scouflaire P, Laux CO, Ducruix S. Lean Flame stabilization with nanosecond plasma discharges in a gas turbine model combustor. In: Proc. ASME Turbo Expo 2023; 2023. GT2023–102621.
[32] Mesquita LCC, Vié A, Zimmer L, Ducruix S. Numerical analysis of flame shape bifurcation in a two-stage swirled liquid burner using Large Eddy Simulation. Proc. Combust. Inst. 2021;38:5971–8. https://doi.org/10.1016/j.proci.2020.06.044.
[33] Cunha Caldeira Mesquita L. Simulation and analysis of the shape, performance, and stability of flames in a two-stage lean-burn aeronautical combustor. Ph.D. Thesis dissertation. CentraleSupélec, Université Paris-Saclay; 2021.
[34] Santhosh R, Miglani A, Basu S. Transition in vortex breakdown modes in a coaxial isothermal unconfined swirling jet. Phys. Fluids. 2014;26:043601. https://doi.org/10.1063/1.4870016.
[35] Rajamanickam K, Basu S. Insights into the dynamics of conical breakdown modes in coaxial swirling flow field. J. Fluid Mech. 2018;853:72–110. https://doi.org/10.1017/jfm.2018.549.
[36] Terhaar S, Reichel TG, Schrödinger C, Rukes L, Paschereit CO, Oberleithner K. Vortex Breakdown Types and Global Modes in Swirling Combustor Flows with Axial Injection. J. Propuls. Power. 2015;31:219–29. https://doi.org/10.2514/1.B35217.
[37] Mesquita LCC, Vié A, Ducruix S. Flashback-induced flame shape transition in a two-stage LPP aeronautical combustor. Proc. Combust. Inst. 2022;000:1–10. https://doi.org/10.1016/j.proci.2022.08.028.
[38] Rusterholtz DL, Lacoste DA, Stancu GD, Pai DZ, Laux CO. Ultrafast heating and oxygen dissociation in atmospheric pressure air by nanosecond repetitively pulsed discharges. J. Phys. D. Appl. Phys. 2013;46:464010. https://doi.org/10.1088/0022-3727/46/46/464010.
[39] Popov NA. Pulsed nanosecond discharge in air at high specific deposited energy: fast gas heating and active particle production. Plasma Sources Sci. Technol. 2016;25:044003. https://doi.org/10.1088/0963-0252/25/4/044003.
[40] IPCC, Climate Change 2007. The Physical Science Basis. Contribution of Working Group I to the Fourth Assessment Report of the Intergovernmental Panl on Climate Change. Cambridge University Press; 2007. https://www.ipcc.ch/report/ar4/wg1/.
[41] Adams S, Miles J, Ombrello T, Brayfield R, Lefkowitz J. The effect of inter-pulse coupling on gas temperature in nanosecond-pulsed high-frequency discharges. J. Phys. D. Appl. Phys. 2019;52:355203. https://doi.org/10.1088/1361-6463/ab27ef.
[42] Blanchard VP, Minesi N, Bechane Y, Fiorina B, Laux CO. Experimental and numerical characterization of a lean premixed flame stabilized by nanosecond discharges. AIAA SciTech Forum 2022;2022:2022–255. https://doi.org/10.2514/6.2022-2255.
[43] Bechane Y. Simulations numériques de la combustion assistée par plasma. Ph.D. Thesis dissertation. CentraleSupélec, Université Paris-Saclay; 2022.

[44] Minesi N. Thermal spark formation and plasma-assisted combustion by nanosecond repetitive discharges. Ph.D. Thesis dissertation. CentraleSupélec: Université Paris-Saclay; 2020.
[45] Del Cont-Bernard D, Guiberti TF, Lacoste DA. Laser induced fluorescence investigation of the chemical impact of nanosecond repetitively pulsed glow discharges on a laminar methane-air flame. Proc. Combust. Inst. 2021;38:6641–9. https://doi.org/10.1016/j.proci.2020.07.097.
[46] Dunn I, Ahmed KA, Leiweke RJ, Ombrello TM. Optimization of flame kernel ignition and evolution induced by modulated nanosecond-pulsed high-frequency discharge. Proc. Combust. Inst. 2021;38:6541–50. https://doi.org/10.1016/j.proci.2020.06.104.